Design, Fabrication, and Evaluation of a Phase-Resolved Partial Discharge Sensor embedded in MV-Class Bushing

Gyeong-Yeol Lee , Nam-Hoon Kim , Dong-Eon Kim , Gyung-Suk Kil * , Sung-Wook Kim

Posted Date: 16 November 2023

doi: 10.20944/preprints202311.1068.v1

Keywords: PRPD sensor; MV-class bushing; accuracy class; phase error; partial discharges

Article

Design, Fabrication, and Evaluation of a Phase-Resolved Partial Discharge Sensor Embedded in MV-Class Bushing

Gyeong-Yeol Lee [1], Nam-Hoon Kim [1], Dong-Eon Kim [1], Gyung-Suk Kil [1,*] and Sung-Wook Kim [2]

[1] Department of Electrical and Electronics Engineering, Korea Maritime and Ocean University, Busan 49112, Korea; priority1@g.kmou.ac.kr (G.-Y. Lee); dom0404@g.kmou.ac.kr (N.-H. Kim); jklfds1003@g.kmou.ac.kr (D.-E. Kim); kilgs@kmou.ac.kr (G.-S. Kil)

[2] Department of Electrical and Electronics Engineering, Silla University, Busan 46958, Korea; number1@silla.ac.kr (S.-W. Kim)

* Correspondence: kilgs@kmou.ac.kr; Tel.: +82-51-410-4893

Abstract: This paper proposes a novel phase-resolved partial discharge (PRPD) sensor embedded in MV-class bushing for high-accuracy insulation analysis. The design, fabrication, and evaluation of a PRPD sensor embedded in MV-class bushing aimed to detect partial discharge (PD) pulses that are phase-synchronized with the applied primary HV signals. A prototype PRPD sensor was composed of a flexible printed circuit board (PCB) with dual-sensing electrodes, utilizing a capacitive voltage divider (CVD) principle for voltage measurement and D-dot principle for PD detection, and a signal transducer with passive elements. A PD simulator was prepared to emulate typical PD defects, i.e., a metal protrusion. The voltage measurement precision of the prototype PRPD sensor was satisfied with the accuracy class of 0.2 specified in IEC 61869-11, as the maximum corrected voltage error ratios and corrected phase errors in 80%, 100%, and 120% of the rated voltage (13.2 kV) were less than 0.2% and 10 minutes, respectively. In addition, the prototype PRPD sensor had good linearity and high sensitivity for PD detection compared with a conventional electrical detection method. According to performance evaluation tests, the prototype PRPD sensor embedded in the MV-class bushing can measure PRPD patterns phase-synchronized with the primary voltage without any additional synchronization equipment or system. Therefore, the prototype PRPD sensor holds potential as a substitute for conventional commercial PD sensors. Consequently, this advancement could lead to the enhancement of power system monitoring and maintenance, contributing to the digitalization and minimization of power apparatus.

Keywords: PRPD sensor; MV-class bushing; accuracy class; phase error; partial discharges

1. Introduction

Insulation degradation in power equipment can be predicted by detecting partial discharge (PD) pulses in the early stages. Various PD sensors have been adapted to detect PD pulses [2,3], including a coupling capacitor, employing the conventional method based on IEC 60270 [1]; and a high-frequency current transformer (HFCT), ultra-high-frequency (UHF) sensor, and an acoustic emission (AE) sensor, based the non-conventional method [2,3]. The conventional detection method produces high-precision PD measurements and shows the output in pC by applying external voltage sources. However, it has the disadvantage of requiring a coupling capacitor installation for quantitative measurements, cannot be used during operation, and limits on-site PD measurements to a maximum measurement frequency of 1 MHz [4–7]. On the other hand, UHF sensors have several advantages, including high sensitivity, good signal-to-noise ratio (S/N), high frequency range (300 kHz to 3 GHz), estimation of fault location, and continuous monitoring. Despite these advantages, UHF measurements have the disadvantage of being unable to calibrate the output magnitude in a unit of pC and are expensive [8–10]. AE sensors are widely used to detect internal defects of electrical power equipment owing to their cheap price and easy installation. The internal fault location can be estimated by calculating the amplitudes and different arrival times of several AE sensors. It cannot be measured in terms of pC, much like with UHF sensors, and must consider the effects of reflections,

 doi:10.20944/preprints202311.1068.v1

attenuations, and scattering of the acoustic waves for the internal structures of the equipment [11–15]. The above PD sensors are selected based on installation conditions and purpose. The most suitable method for insulation diagnosis is phase-resolved partial discharge (PRPD) analysis, which includes the phase angle ($\emptyset$), PD magnitude (q), and the number of PD pulses (n) over a period within one cycle of the applied voltage source [16,17].

An accurate measurement of system voltage signals is critical to improve the safety and reliability of power equipment. The voltage signals obtained by various instruments, including iron-core-type potential transformers (PTs), capacitive potential transformers (CPTs), and resistive potential transformers (RPTs), have a critical role in the operation of protective relays to counter abnormal voltage surges. The iron-core-type PT requires a significantly large installation space due to its iron core and copper wire components, and can be susceptible to external transients when connected directly between primary and secondary circuits [18]. Capacitive potential transformers must be connected to high-input impedance instruments, typically exceeding several megohms. Alternatively, an impedance transformer must be used to match the input and output impedance between the CPT and the instrument. While these instruments can be used effectively within a narrow frequency band corresponding to commercial frequencies, their accuracy can be compromised if the voltage signal is contaminated with high-frequency noise components [19,20]. Therefore, the development of high-precision voltage measurement instruments with broadband frequency capability is essential. To address the challenges associated with ensuring an adequate insulation distance for direct connections to primary high-voltage conductors, as well as issues such as magnetic saturation, deformation of internal cores, and the need for significant installation space, a novel voltage measurement method for low-power voltage transformers (LPVTs) has been the subject of recent research. This need prompted the International Electrotechnical Commission (IEC) to publish IEC 61869-11 [21], relevant to low-power voltage transformers (LPVTs) using passive elements, to replace IEC 60044-7 [22], which is currently applied to electronic voltage transformers (EVTs). This is intended for connection to stand-alone merging units (SAMUs) or metering devices according to IEC 61869-13 [23].

Wagoner et al. [24] diagnosed the current and voltage output signals in the vacuum section of a 20 MA 3 MV pulsed power accelerator using differential D-dot and B-dot sensors with a common mode for noise rejection. Wang and colleagues [25] developed voltage transformers using the basis of a differential D-dot sensor. They experimented and simulated the designed D-dot probe sensor for the verification of measurement accuracy. Kim et al. [26] developed an electronic voltage transformer (EVT) with an accuracy class of 0.2 using a D-dot sensor. They showed that the prototype EVT can accurately detect voltage signals up to the 3rd, 5th, and 7th harmonics at a commercial frequency of 60 Hz upon employing a non-contact voltage measurement method.

Wang and colleagues [27] investigated an electronic voltage transformer with a self-integral D-dot sensor using the D-dot principle for high-voltage signal measurement. They found that the D-dot sensor operates self-integrated modes with excellent phase frequency characteristics by applying parallel and differential structures of multiple electrodes. Yao and colleagues [28] proposed a compensation method that improves the accuracy of output signals by minimizing the offset due to the integrated circuit of the D-dot electric field sensor. A mathematical method from this study was proposed to reduce the offset value by the integration circuit. However, in the view of condition monitoring, the proposed devices and methods cannot detect abnormal pulses from internal defects because they are mainly designed to measure the system voltage signals.

Hussain et al. [29] studied the online monitoring sensor, capturing the abnormal electrical fault signals generated from an internal arc for medium-voltage (MV) switchgears based on a differential D-dot principle. Hussain and colleagues [30] compared the detection characteristics of the Rogowski coil, loop antenna, HFCT, and D-dot sensor in air-insulated switchgears, and discovered that the Rogowski coil sensor and D-dot sensor are more suitable for the PD measurements due to their high signal-to-noise ratio (S/N). Rostaghi-Chalaki and colleagues [31] investigated the output characteristics of a D-dot and B-dot measuring the DC PD pulses propagating through the transmission line (TL) using the electromagnetic (EM) field principle. They found that the apparent

 doi:10.20944/preprints202311.1068.v1

discharge measured by the EM field sensors were almost identical to the reference PD pulse measured by the oscilloscope. Jin and colleagues [32] studied the measurement of the transient-pulsed electromagnetic field using a D-dot sensor, and outlined a compensation system for the recovery of the incident E-field to improve the dynamic characteristics. Although the sensors are designed to detect PD pulses, they are not suitable for diagnostic devices because the signals cannot be analyzed using a phase-resolved partial discharge (PRPD) method due to the absence of the voltage phase information.

Information about the phase distribution of the PD pulses is an essential parameter for PD diagnosis of high-voltage power equipment. However, it is difficult to obtain the exact phase angle and magnitude of the PD pulses phase-synchronized with the applied high voltage because the detection methods do not inherently indicate at which phase the PD pulse occurred. Therefore, many studies have been conducted regarding how to obtain the PD pulses phase-synchronized with the applied high voltage or the zero-crossing point of the applied high voltage. Kim et al. [33] suggested a possible diagnosis technique of unknown phase-shifted PD signals for GISs. The new diagnosis method utilized the shapes, distribution ranges, density, and peak values of the PD pulses and could classify internal defect types and noises without phase distribution information of the applied voltage. Lee and colleagues [34] developed a neural network algorithm to discriminate phase-shifted PRPD patterns. They proposed a new method which was able to convert the fundamental phase-shifted parameters, such as phase angle, magnitude, and the number of PD pulses, to standardized parameters by applying the neural network algorithm method. However, there are limitations to setting criteria for determining internal defects, as their identification relies on the knowledge and experience of the engineer. Therefore, the development of techniques for the acquisition of accurate phase angles of applied voltage signals for insulation diagnosis remains necessary.

To address these limitations, this paper proposes a PRPD sensor embedded in MV-class bushing, capable of detecting phase-synchronized PD pulses through precise measurements of the primary HV signal. The prototype PRPD sensor demonstrated a voltage measurement accuracy that was satisfied with an accuracy class of 0.2 by analyzing the error ratio and phase error according to the test guidelines in IEC 61869-11. Furthermore, the PRPD sensor had good linearity and sensitivity of PD detection by comparing the output magnitude and PRPD pattern detected using the conventional electrical detection method specified in IEC 60270. It is expected that the prototype PRPD sensor can minimize the installation area of the epoxy insulation and help precise the insulation diagnosis for acquiring the PD pulses phase-synchronized with the applied signal.

2. Design and Fabrication

Detecting PD pulses phase-synchronized with the applied voltage signals is the most important technology to identify and distinguish internal defects. The prototype PRPD sensor embedded in the MV-class bushing consists of dual-sensing electrodes and signal transducers for voltage signal measurement and PD detection.

2.1. PRPD sensor embedded in a bushing

Figure 1 shows a configuration and photograph of the prototype PRPD sensor embedded in MV-class bushing. The PRPD sensor was designed using a non-contact detection method. The dual-sensing electrodes consisted of a voltage transformer (VT) for voltage signals with a commercial frequency band (around 60 Hz) and a D-dot sensor for PD pulses with high-frequency ranges, respectively. The electrodes were installed on a flexible PCB to encircle around the HV conductor and minimize external environmental impacts such as shock or vibration.

Preprints (www.preprints.org) | NOT PEER-REVIEWED | Posted: 16 November 2023 doi:10.20944/preprints202311.1068.v1

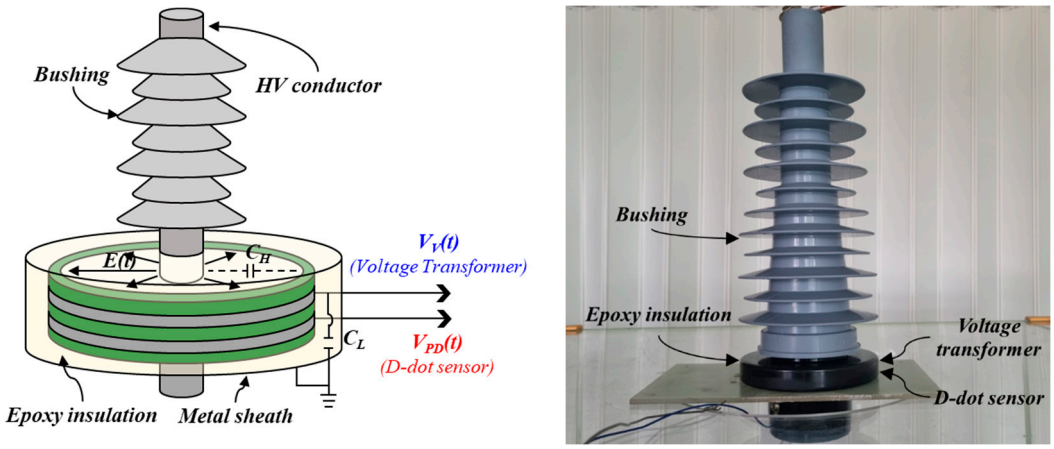

(**a**) (**b**)

Figure 1. The prototype PRPD sensor: (**a**) configuration; and (**b**) photograph.

The capacitive divider principle was applied for the design and fabrication of the VT sensor as this is did not allow for derivative output signals according to IEC 61869-11. The output voltage of the VT, $V_V(t)$, is proportional to the primary HV signal, $U_P(t)$, and it can be calculated using Equation (1):

$$V_V(t) = \frac{C_H}{C_H + C_L + C_V} \times U_P(t) \quad (1)$$

where C_H is a HV stray capacitor between the HV conductor and the sensing electrode of the VT, C_L is a LV capacitor between the sensing electrode and a grounded metal sheath, and C_V is a capacitor for controlling a transformation ratio in parallel with the LV capacitor. For the study outlined in this paper, the rated transformation ratio of the prototype PRPD sensor was set to 10,000:1.

Contrastingly, in accordance with the Gaussian law [20,21,34], the output voltage of the D-dot sensor $V_{PD}(t)$ is proportional to the primary derivation value of the incident electrical field $\vec{E}$, and can be calculated using Equation (2):

$$V_{PD}(t) = R_m \cdot S_{eq} \cdot \varepsilon \cdot \frac{d\vec{E}(t)}{dt} \quad (2)$$

where R_m is an output impedance of V_{PD}, S_{eq} is an equivalent area of the closed surface of the D-dot electrode, ε is the permittivity of an epoxy insulation, and $\vec{E}$ is the magnitude of the incident electrical field generated by the HV conductor. Since the duration time of PD pulses is less than a few nanoseconds, they do not require the application of a restoration process.

Table 1 shows the geometric parameters of the prototype PRPD sensor outlined in this paper. A high glass transition temperature (T_g-type) PCB was used to prevent deformation by heat generated during the epoxy molding process. The PRPD sensor was housed within an aluminum alloy metal sheath for protection from external electrical fields such as shocks, vibration, or surges. The new application of the PRPD sensor was designed and fabricated with good advantages such as good linearity, high sensitivity, low manufacturing cost, and installation location agnostic.

Table 1. Geometric parameters of the PRPD sensor.

Parameter		Value
Diameter		Φ 160 mm
Height		12 mm
Sensing electrodes (Voltage and PD)	Width	3 mm
	Thickness	1 oz
Insulation layer		0.2 mm

Preprints (www.preprints.org) | NOT PEER-REVIEWED | Posted: 16 November 2023 doi:10.20944/preprints202311.1068.v1

Dielectric constant (ε_s)	4.7

2.2. Signal Transducer

The output signals from the VT and D-dot sensor of the PRPD sensor were connected with each signal transducer, as shown in Figure 2. In a signal transducer for the VT, C_V as the transformation ratio control capacitor and R_{m1} for impedance matching were installed in parallel with C_L, the LV capacitor of the VT. The magnitude of C_L was fixed by the insulation material and geometric parameters including thickness, length, and width. Therefore, based on Equation (1), the magnitude of C_V should be chosen carefully to satisfy the high-accuracy measurement specified in IEC 61869-11. The output resistance, R_{m1}, was set to 2 MΩ for impedance matching with the measuring instrument. A gas discharge tube (GDT) was installed at the front of the transducer circuit to protect from unexpected surges during the experiment.

On the other hand, in a signal transducer for the D-dot sensor, C_{PD} and L_{PD} were installed for operating as high-pass filters (HPFs) to obtain PD pulses with a high frequency range. The output resistor, R_{m2}, was set to 50 Ω and was connected in parallel with L_{PD} for impedance matching with the measurement instrument. The cut-off frequency was about 63 kHz. The gain of the transducer was 1 in the frequency range above 100 kHz, so the output of the PD pulses is directly proportional to the magnitude of the PD pulse.

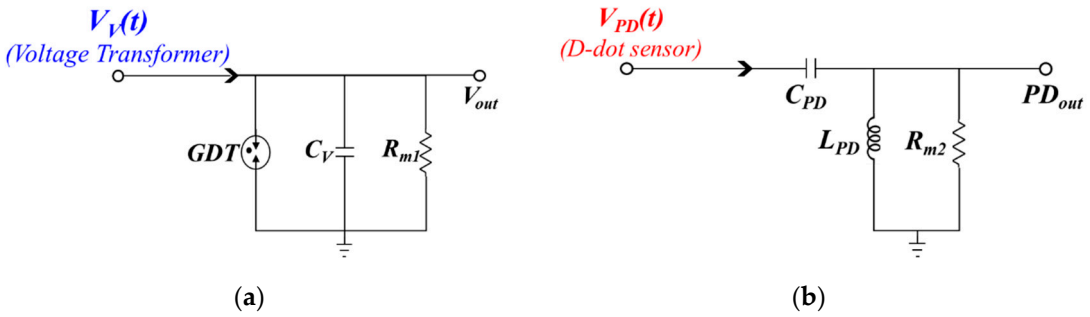

Figure 2. Configuration of the signal transducers: (**a**) voltage signals; and (**b**) PD pulses.

3. Experiment and Method

3.1. PD Simulator

PD pulses are important indicators of insulation deterioration analysis because they occur at an early stage inside the electrical equipment. Therefore, internal defects can be predicted by detecting PD pulses before their breakdown. Despite the scientific efforts of manufacturers, installers, and operators to prevent the introduction of foreign objects and contaminants during the manufacturing, installation, and operation phases, small defects are still detected in electrical equipment. These defects can lead to insulation degradation.

Throughout the manufacturing process or during operation, the existence of imperfections or irregularities in materials, welding, or assembly can lead to the formation of sharp metal protrusions. When the electrical field is concentrated at the apex of these metal protrusions, it triggers a corona-type PD. Typically, PD pulses originate from a specific location on the metal protrusion, where it be on an enclosure of electrical equipment. Figure 3 shows the PD simulator of a metal protrusion defect. The metal protrusion was fabricated by using a spherical conductor with a diameter of 30 mm as the HV side and a needle with a radius of curvature of 10 um on a flat electrode, with a diameter of 80 mm as the ground plate. The needle electrode represents a micro-size metal protrusion on the enclosure of the power apparatus. A spherical conductor with a diameter of 25 mm was installed to prevent the electric field from concentrating on the high-voltage connection.

Preprints (www.preprints.org) | NOT PEER-REVIEWED | Posted: 16 November 2023 doi:10.20944/preprints202311.1068.v1

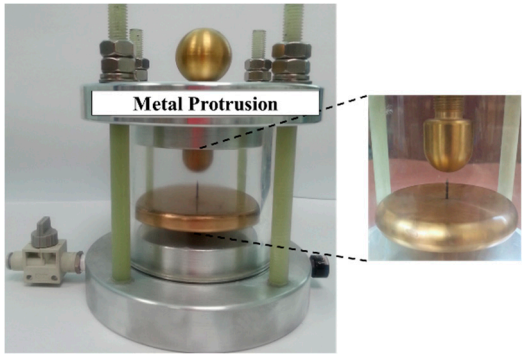

Figure 3. Photograph of an artificial PD simulator.

3.2. Experimental Setup

Figure 4 shows an experimental setup for evaluating the accuracy of voltage measurement according to IEC 61869-11 requirements and PD detection of the prototype PRPD sensor. A dry-type transformer with a maximum output of 100 kV was used to apply a high voltage, and was controlled by an induction-type automatic voltage regulator (IVR). A HV divider with an accuracy class of 0.2 and a ratio of 1,000:1 was connected to compare the output of the PRPD sensor. A 50 Ω non-inductive resistor (NIR) was installed between the PD simulator and the ground as a conventional electrical detection method according to IEC 60270. All signals from the PRPD sensor, HV divider, and the 50 Ω NIR were recorded using a digital storage oscilloscope (DL750P, YOKOGAWA), with a sampling rate of 10 MS/s. The HV Tr., IVR, HV divider, PD simulator, and measuring devices were grounded to avoid an unexpected electrical potential difference. The level of background noise was less than 3 mV (measured using the prototype PRPD sensor) and 2 mV (measured using a 50 Ω NIR), respectively, in the experiment.

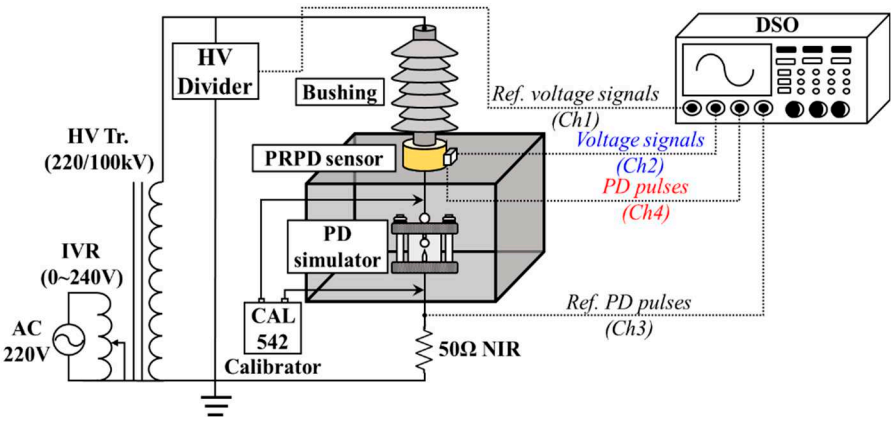

(**a**)

(**b**)

Preprints (www.preprints.org) | NOT PEER-REVIEWED | Posted: 16 November 2023 doi:10.20944/preprints202311.1068.v1

Figure 4. Experimental setup: (**a**) schematic diagram; and (**b**) photograph.

4. Performance Evaluation

4.1. Voltage Measurement

To assess the sensitivity and accuracy of the voltage measurement, 80%, 100%, and 120% of the rated voltage (13.2 kV) were applied according to the test guideline in IEC 61869-11. Figure 5 shows example waveforms and phase errors of the applied voltage, and the PRPD sensor at each voltage level. The voltage waveforms were captured for six cycles to compare the average voltage levels. In addition, the phase errors were confirmed by analyzing each zero-crossing (ZC) point of the waveforms of the applied voltage and the PRPD sensor.

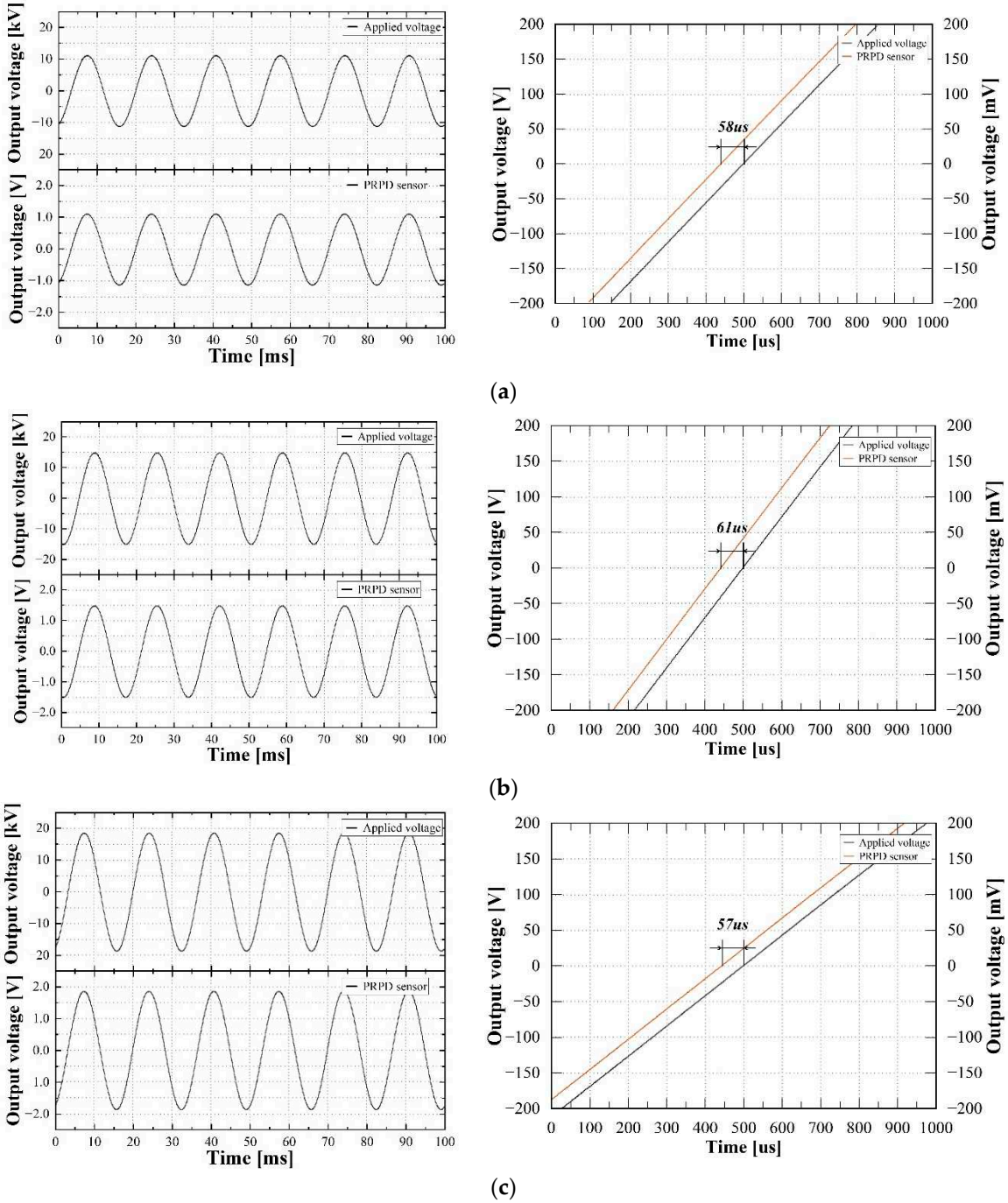

Figure 5. Example waveforms and phase errors: (**a**) 80%; (**b**) 100%; and (**c**) 120%.

Preprints (www.preprints.org) | NOT PEER-REVIEWED | Posted: 16 November 2023 doi:10.20944/preprints202311.1068.v1

The deviations of the output voltages and phase errors between the applied voltage and the PRPD sensor can be adjusted by the correction factor CF_U within a range of 0.900 to 1.100 and phase offset correction $\varphi_{0\,cor}$ within a range of 300 min (5 degrees or 231 us). The correction factor CF_U and phase offset correction $\varphi_{0\,cor}$ of the prototype PRPD sensor were set to 1.000 and 76 minutes, respectively. The corrected voltage ratio error $\varepsilon_{cor\,U}$ and corrected phase error $\varphi_{e\,cor}$ were calculated using Equations (3) and (4), respectively:

$$\varepsilon_{cor\,U}(\%) = \frac{CF_U \cdot K_r \cdot V_L - V_H}{V_H} \times 100 \quad (3)$$

$$\varphi_{e\,cor} = \varphi_S - \varphi_P - \varphi_{cor\,\varphi 0} \quad (4)$$

where K_r is the rated transformation ratio of 10,000, V_H is the applied voltage, V_L is the output voltage of the PRPD sensor, φ_S is the phase angle of the PRPD sensor, and φ_P is the phase angle of the applied voltage.

Table 2 shows the corrected error ratio $\varepsilon_{cor\,U}$ and corrected phase error $\varphi_{e\,cor}$ at each applied voltage, i.e., 80%, 100%, and 120% of the rated voltage, calculated using Equations (3) and (4). The maximum values of the voltage ratio error and the phase errors were 0.166% and + 3.06 minutes, respectively. From the voltage measurement test, the PRPD sensor could meet the accuracy class of 0.2, as specified in IEC 61869-11, because the voltage ratio error and phase error at each applied voltage did not exceed 0.2% and 10 minutes.

Table 2. Accuracy test results of the PRPD sensor.

Voltage level	Applied voltage V_H [kV]	PRPD sensor V_L [V]	Corrected error ratio $\varepsilon_{cor\,U}$ [%]		Corrected phase error $\varphi_{e\,cor}$ [min]	
			Measured value	Accuracy class of 0.2	Measured value	Accuracy class of 0.2
$0.8U_P$	10.561	1.056	0.001	0.2	- 0.83	10
$1.0U_P$	13.204	1.322	0.126		+ 3.06	
$1.2U_P$	15.803	1.583	0.166		- 2.13	

4.2 PD Detection

Before the PD detection experiment, a calibration test was conducted to evaluate the linearity of the prototype PRPD sensor using the PD simulator. Artificial calibration pulses of 10 pC, 20 pC, 50 pC, and 100 pC with a rising time of tens of nanoseconds were injected into the PD simulator using a calibrator (CAL 1A, Power Diagnostix Systems GmbH). The PD simulator was filled with SF_6 of the gas pressure at 0.5 MPa. Figure 6 shows the average output voltage detected by the PRPD sensor and the conventional electrical detection method in accordance with the calibration pulses. Each output voltage of the 50 Ω NIR and PRPD sensor was recorded five times to calculate their average values. The calibration test confirmed that the output of the prototype PRPD sensor had linearity with respect to the calibration inputs and was more sensitivity than the conventional method.

Preprints (www.preprints.org) | NOT PEER-REVIEWED | Posted: 16 November 2023 doi:10.20944/preprints202311.1068.v1

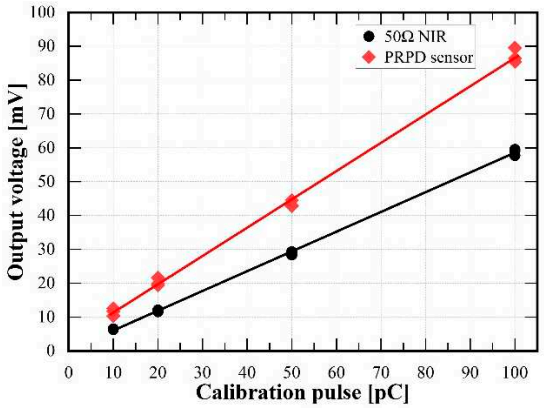

Figure 6. Output voltage for the calibration pulse.

Figure 7 shows a typical single PD pulse generated from the metal protrusion defect measured by the prototype PRPD sensor at 4 kV, along with its fast Fourier transform (FFT). The rising time, falling time, and pulse width were analyzed by calculating the average values of 10 single PD pulses, and they were 145 ns, 116 ns, and 202 ns, respectively. The main frequency range of the single PD pulse was distributed between 27 MHz to 47 MHz, and the maximum frequency range with the highest magnitude was 28 MHz.

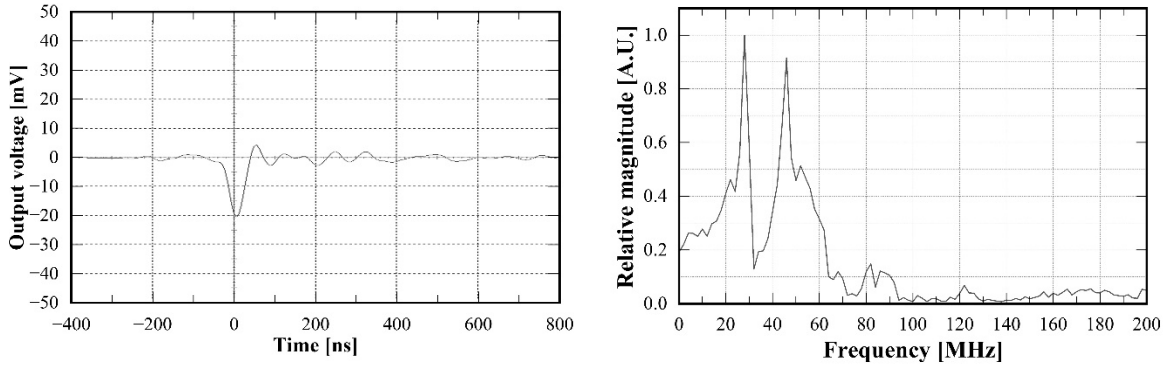

(**a**) (**b**)

Figure 7. Example waveform: (**a**) single pulse; and (**b**) fast Fourier transform (FFT).

Figure 8 shows example PRPD patterns measured by the prototype PRPD sensor and 50 Ω NIR at the same applied voltage of 4 kV. The PD pulses generated from the PD simulator accumulated for 1 minute. The applied voltage signal of the prototype PRPD sensor and the 50 Ω NIR was measured by using the VT of the PRPD sensor and HV divider, respectively. The PD pulses of the PRPD sensor were distributed at the phase angle of 26° to 105°, and 221° to 276°. On the other hand, the PD pulses of the 50 Ω NIR were distributed at the phase angle of 25° to 106° and 220° to 269°. From the comparison of the phase distributions detected by each sensor, the PRPD sensor and 50 Ω NIR, there were no differences between them. In addition, the shape of the PRPD pattern detected by using the prototype PRPD sensor had a similarity to that of the 50 Ω NIR. According to the PRPD measurement, the prototype PRPD sensor could detect the PRPD patterns phase-synchronized with the applied voltage signals without any additional devices.

Preprints (www.preprints.org) | NOT PEER-REVIEWED | Posted: 16 November 2023 doi:10.20944/preprints202311.1068.v1

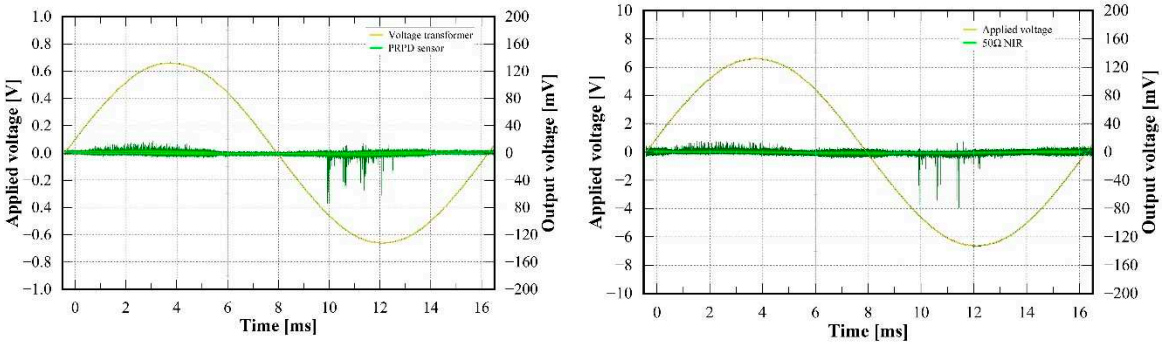

(**a**) (**b**)

Figure 8. Comparison of PRPD patterns detected by: (**a**) PRPD sensor; and (**b**) 50 Ω NIR.

5. Conclusions

Many PD detection techniques have been extensively studied to diagnose the insulation degradation in power equipment, but conventional PD sensors are hampered by the drawback of necessitating an independent device or system for the synchronous detection of PD patterns alongside the applied high voltage signal. Detecting the PD pulses phase-synchronized with the applied voltage signals is a critical issue due to the PD pulses depending on the magnitude and phase of the applied voltage. This study proposed a novel PRPD sensor embedded in MV-class bushing which could detect PD pulses phase-synchronized with applied voltage signals for the insulation deterioration diagnosis of electrical power equipment. The prototype PRPD sensor consisted of dual-sensing plates fabricated on the insulated flexible PCB and the signal transducer for calibrating the outputs of the voltage signals and PD pulses. The CVD and D-dot principles were applied to the voltage measurement and PD detection, respectively. In order to assess the efficacy of the suggested PRPD sensor, the experimental system was established. The voltage measurement accuracy of the PRPD sensor was evaluated in accordance with the testing standards specified in IEC 61869-11. Furthermore, the linearity and sensitivity of PD detection were compared with conventional electrical sensing techniques. The experimental results are summarized below:

A. Voltage measurement

Evaluation of voltage measurement accuracy was focused on the deviation of the output magnitude and phase among the applied voltage and PRPD sensor. The designed rated transformation ratio was 10,000:1. The correction factor and corrected phase offset were set to be 1.000, and 76 minutes. The maximum corrected error ratio and corrected phase error were 0.126% and + 3.06 minutes, respectively, and they were commonly detected at 100% of the rated voltage.

B. PD detection

The prototype PRPD sensor was linear to the artificial PD calibration pulses. Alongside that, the outputs of the PRPD sensor were approximately 1.5 times larger than those of the conventional electrical detection method via a 50 Ω NIR. Regarding the time and frequency domains, the rising time of the PD pulse was relatively longer than the falling time, and the maximum magnitude was analyzed in the frequency range of about 24 MHz. The prototype PRPD sensor was able to detect the PRPD patterns phase-synchronized with the applied voltage signal successfully. The phase ranges of the PD pulses detected by the PRPD sensor were almost the same as those detected using the conventional method.

From the experimental results, it is expected that the proposed PRPD sensor holds potential as a viable alternative to conventional PD sensors due to its usefulness in diagnosing internal degradation. Figure 9 shows a flowchart of the proposed PRPD measurement method phase-synchronized with the applied voltage signal, as proposed in this study. Further research is required as more PD characteristics need to be analyzed for the precise analysis of PD defects. Based on these considerations, additional PD characteristics of various types of PD defects, such as epoxy voids,

Preprints (www.preprints.org) | NOT PEER-REVIEWED | Posted: 16 November 2023 doi:10.20944/preprints202311.1068.v1

delamination, cracks, metal suspension, and metal particles in the enclosure, should be investigated, and further research should be conducted on identifying PD defect types and identifying PD sources in the future.

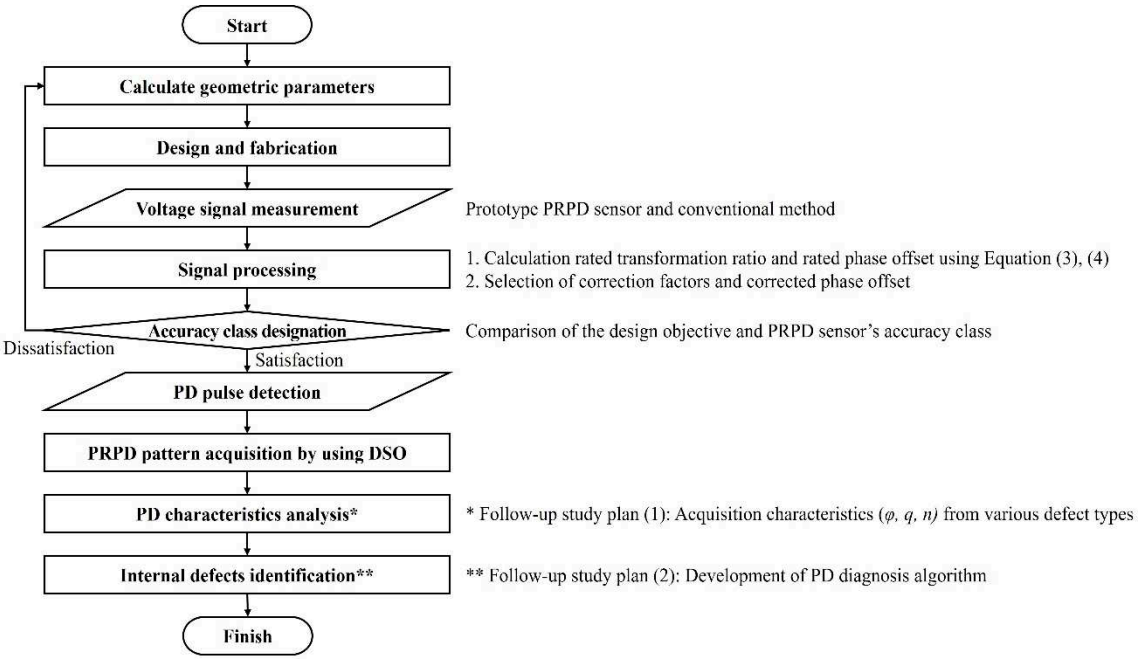

Figure 9. Flowchart of the PRPD measurement method phase-synchronized with applied voltage.

Author Contributions: G.-Y.Lee, and N.-H.Kim conceived and designed the experiments; G.-Y.Lee, N.-H.Kim, and D.-E.Kim performed the experiments; N.-H.Kim and D.-E.Kim generated the raw data and G.-Y.Lee and S.-W.Kim analyzed the data; G.-Y.Lee, D.-E.Kim, and S.-W.Kim wrote the paper; G.-S.Kil was the supervisor of this work and provided insight and technical expertise to improve the quality of this study. All authors have read and agreed to the published version of the manuscript.

Funding: This work was funded by the Technology Innovation Program (No. 20010965, Development of Electronic Current Voltage Transformer and Spacer based on eco-friendly solid insulation) funded by the Ministry of Trade, Industry & Energy (MOTIE) and the Korea Evaluation Institute of Industrial Technology (KEIT) of the Republic of Korea.

Conflicts of Interest: The authors declare no conflict of interest.

References

1. IEC 60270: High-Voltage Test Techniques – Partial Discharge Measurements; 2000.
2. CIGRE WG D1.33; High-voltage On-site Testing with Partial Discharge Measurement. CIGRE Tech. Broch. 2012, 502.
3. Chai. H.; Phung. B.T.; Mitchell. S.; Application of UHF Sensors in Power System Equipment for Partial Discharge Detection: A Review. *Sensors* **2019**, 19, 1029. https://doi.org/10.3390/s19051029
4. F. H. Kreuger; Partial Discharge Detection in High Voltage Equipment. *Butterworth* 1989, 129.
5. Liu. J.; Zhang. G.; Dong. J.; Wang. J. Study on Miniaturized UHF Antennas for Partial Discharge Detection in High-Voltage Electrical Equipment. *Sensors* **2015**, *15*, 29434-29451. https://doi.org/10.3390/s151129434
6. CIGRE WG D1.37; Guidelines for Partial Discharge Detection using Conventional (IEC60270) and Unconventional Methods. *CIGRE Tech. Broch*. **2016**, 662.
7. M. Wu; H. Cao; J. Cao; H. L. Nguyen; J. B. Gomes; S. P. Krishnaswamy; An overview of state-of-the-art partial discharge analysis techniques for condition monitoring. *IEEE Electr. Insul. Mag.* **2015**, *31*, 22-35. https://doi.org/10.1109/MEI.2015.7303259
8. Wang. X.; Li. X.; Rong. M.; Xie. D.; Ding. D.; Wang. Z.; UHF Signal Processing and Pattern Recognition of Partial Discharge in Gas-Insulated Switchgear Using Chromatic Methodology. *Sensors* **2017**, *17*, 177. https://doi.org/10.3390/s17010177
9. Schichler. U.; Koltunowicz. W.; Gautschi. D.; Girodet. A.; Hama. H.; Juhre. K.; Lopez-Roldan. J.; Okabe. S.; Neuhold. S.; Neumann. C.; Pearson. J.; Pietsch. R.; Riechert. U.; Tenbohlen. S.; UHF Partial Discharge

Detection System for GIS: Application Guide for Sensitivity Verification. *IEEE Trans. Dielectr. Electr. Insul.* **2016**, *23*, 1313-1321. https://doi.org/10.1109/TDEI.2015.005543
10. CIGRE WG B3.24; Benefits of PD diagnosis on GIS condition assessment. *CIGRE Tech. Broch.* **2017**, 674.
11. S.W. Kim; N.H. Kim; D.E. Kim; T.H. Kim; D.H. Jeong; Y.H. Chung; G.S. Kil; Experimental Validation for Moving Particle Detection Using Acoustic Emission Method. *Energies* **2021**, *14*, 8516. https://doi.org/10.3390/en14248516
12. L. Lundgaard; B. Skyberg; A. Schei; A. Diessner; Method and instrumentation for acoustic diagnoses of GIS. *CIGRE session,* **2000**, *15*.
13. M. Mondal; G. B. Kumbhar; Partial Discharge Localization in a Power Transformer: Methods, Trends, and Future Research. *IETE Technical Review*, **2017**, *34*, 504-513. https://doi.org/10.1080/02564602.2016.1209436.
14. de Castro, B.A.; dos Santos, V.V.; Lucas, G.B.; Ardila-Rey, J.A.; Riehl, R.R.; Andreoli, A.L. A Comparative Analysis Applied to the Partial Discharges Identification in Dry-Type Transformers by Hall and Acoustic Emission Sensors. *Sensors* **2022**, 22, 1716. https://doi.org/10.3390/s22051716
15. Sikorski, W.; Wielewski, A. Low-Cost Online Partial Discharge Monitoring System for Power Transformers. *Sensors* **2023**, 23, 3405. https://doi.org/10.3390/s23073405
16. G.C. Shin; S.W. Kim; G.S. Kil; Comparison between the PD Characteristics of g3 and Dry Air for Gas-Insulated Switchgears. *Energies* **2022**, *15*, 7043, https://doi.org/10.3390/en15197043.
17. R. Bozzo; L. Centurioni; F. Guastavino; Measuring the Endurance of Films in Partial Discharges. *IEEE Trans Dielectr. Electr. Insul*. **1993**, 28, 1050-1056. https://doi.org/10.1109/14.249378
18. Z. Lu; Z. Li; S. Lu; M. Xu; W. Liu; Fault Mechanism Analysis of Voltage Transformer Caused By Iron Core Saturation. *2022 IEEE 6th Advanced Information Technology, Electronic and Automation Control Conference (IAEAC)* **2022**, Beijing, China, 856-859. https://doi.org/10.1109/IAEAC54830.2022.9929771
19. Y. Xiao; J. Fu; B. Hu; X. Li; C. Deng; Problems of voltage transducer in harmonic measurement. *IEEE Trans. Pow. Deliv.* **2004**, *19*, 1483-1487. https://doi.org/10.1109/TPWRD.2004.829947
20. Mingotti. A; Costa. F; Pasini. G; Peretto. L; Tinarelli. R; Modeling Capacitive Low-Power Voltage Transformer Behavior over Temperature and Frequency. *Sensors* **2021**, *21*, 1719. https://doi.org/10.3390/s21051719
21. IEC 61869-11: Instrument transformers - Part 11: Additional requirements for low-power passive voltage transformers, **2017**.
22. IEC 60044-7: Instrument transformers - Part 7: Electronic voltage transformers, **1999**.
23. IEC 61869-13: Instrument transformers - Part 13: Stand-alone merging unit (SAMU), **2021**.
24. Wagoner, T. C. at el; Differential-output B-dot and D-dot monitors for current and voltage measurements on a 20-MA, 3-MV pulsed-power accelerator. *Physical Review Special Topics - Accelerators and Beams* **2008**, *11*, 100401. https://doi.org/ 10.1103/PhysRevSTAB.11.100401
25. J. Wang; S. Ban; Y. Yang; A Differential Self-Integration D-Dot Voltage Sensor and Experimental Research. *IEEE Sensors J*. **2015**, *7*, 3846-3852. https://doi.org/10.1109/JSEN.2015.2399413.
26. N.H. Kim; D.E. Kim; S.W. Kim; J.H. Kim; G.S. Kil; Development of Electronic Voltage Transformer for Electric Rolling Stocks. J. *Korean Soc. Railw.* **2023**, 26, 445-453. https://doi.org/10.7782/JKSR.2023.26.6.445.
27. Wang. J.; Gao. C.; Yang. J.; Design, Experiments and Simulation of Voltage Transformers on the Basis of a Differential Input D-dot Sensor. *Sensors* **2014**, *14*, 12771-12783. https://doi.org/10.3390/s140712771
28. L. Yao; J. Huang; N. Kang; T. Shen; D. Liu; F. Zhang; H. Sun; Compensation of the offset in numerical integration of a D-dot sensor measurement. *Proceedings of 2014 3rd Asia-Pacific Conference on Antennas and Propagation*, Harbin, China, **2014**, 898-901. https://doi.org/10.1109/APCAP.2014.6992645.
29. G. A. Hussain; M. Shafiq; M. Lehtonen; M. Hashmi; Online Condition Monitoring of MV Switchgear Using D-Dot Sensor to Predict Arc-Faults. *IEEE Sensors J.* **2015**, *15*, 7262-7272. https://doi.org/10.1109/JSEN.2015.2474122
30. G. A. Hussain; G, Amjad; A, A, Zaher; D, Hummes; M, Safdar; M, Lehtonen; Hybrid Sensing of Internal and Surface Partial Discharges in Air-Insulated Medium Voltage Switchgear. *Energies* **2020**, *13*, 1738. https://doi.org/10.3390/en13071738
31. M. Rostaghi-Chalaki; K. Yousefpour; J. P. Donohoe; M. Kurum; C. Park; J. Klss; Design of Transmission Line and Electromagnetic Field Sensors for DC Partial Discharge Analysis. *IEEE Trans Dielectr. Electr. Insul.,* **2020**, *27*, 2138-2146. https://doi.org/1109/TDEI.2020.009003
32. Jin. M.; Li. H.; Liu. S.; Identification and Compensation for D-Dot Measurement System in Transient Electromagnetic Pulse Measurement. *Sensors* **2022**, 22, 8538. https://doi.org/10.3390/s22218538
33. S.W. Kim; J.R. Jung; Y.M. Kim; G.S.Kil; G. Wang; New Diagnosis Method of Unknown Phase-shifted PD Signals for Gas Insulated Switchgears. *IEEE Trans Dielectr. Electr. Insul*. **2018**, 25, 102-109. https://doi.org/10.1109/TDEI.2018.006739
34. J.H. Lee; N. Hozumi; T. Okamoto; Discrimination of phase-shifted partial discharge patterns by neural network using standardization method. *Proceedings of 1994 IEEE International Symposium on Electrical Insulation* **1994**, Pittsburgh, USA, 314-317. 10.1109/ELINSL.1994.401504.

 doi:10.20944/preprints202311.1068.v1